Mem. S.A.It. Vol. 76, 378

Memorie della

Time-dependent shocks and line emission in Herbig-Haro jets

S. Massaglia[1], A. Mignone[2] and G. Bodo[2]

[1] Dipartimento di Fisica Generale, Universitá di Torino, via Pietro Giuria 1, 10125 Torino
e-mail: massaglia@ph.unito.it
[2] Osservatorio Astronomico di Torino, Strada Osservatorio 20, 10025 Pino Torinese, Italy

Abstract. Herbig-Haro jets cool radiatively in a very effective way. Nevertheless, high resolution observations show that temperature along the jet remains above 5,000 K and ionization above 10%, showing a tendency to increase in some regions. Therefore one needs to examine whether there are mechanisms that can successfully balance radiative losses. In this paper we assume that the fraction of the jet that emits the observed spectral lines is small, filling factor ∼1%, and consider shock dissipation as possible excitation mechanism. We carry out time-dependent numerical simulations of planar perturbations that evolve into shocks and compare the results with observations.

Key words. Hydrodynamics – stars: early-type – ISM: jets and outflows

1. Introduction

Herbig-Haro jets can be observed at very high spatial resolution by HST, and with the next generation of ground based optical telescopes such as VLTI the angular resolution capabilities will be boosted from the actual fraction of arcsecond up to the milliarcsecond range. It will soon be possible to look into the very first part of the jet as it emerges from the accretion disk or from the reflection nebula and resolve the jet in its radial extent. The jets of HH 30 (see Bacciotti et al. 1999) and DG Tau (see C. Lavalley-Fouquet et al. 2000, Bacciotti et al. 2004) are particularly good candidates for high resolution studies of the evolution of the physical parameters along the initial fraction of the jet, i.e. up to $\sim 600 - 1,000$ AU. These jets lie almost to the plane of the sky, the dust torii that surround the central star are natural coronographs that allow to observe the very first phases of the jet.

These observations typically show that the observed emission lines and the behavior of temperature, ionization and density along the jet, as derived from observations, are incompatible with a freely cooling jet. Various heating processes have been proposed in the literature, such as ambipolar diffusion (see Garcia et al. 2001), photoionization by soft x-rays from the TTauri star (e.g. Shang et al. 2002) and mechanical heating (O'Brien et al. 2003, Shang et al. 2002, for X-wind jets). These estimates where carried out for steady-state jet models and pointed out that mechanical heating was the most effective in reproducing the observations. The idea of tapping a small fraction of

Send offprint requests to: S. Massaglia
Correspondence to: via Pietro Giuria 1, 10125 Torino

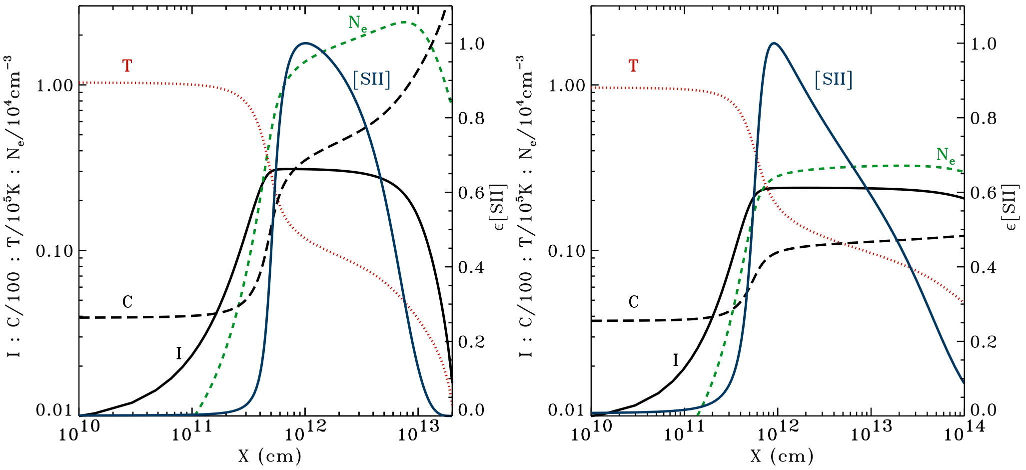

Fig. 1. Left panel: Spatial evolution of the post-shock temperature (label T), electron density (N_e), compression ratio (C), ionization fraction (I) and emissivity in the [$S\,II$] line, scaled to the maximum value. The (stationary) shock velocity is $V_\mathrm{s} = 60$ km s^{-1} and the upstream values are temperature $T_0 = 2,000$ K, density $N_0 = 1,000$ cm^{-3}, ionization fraction $I = 0.01$ and magnetic field $B_0 = 0$. Right panel: The same as in the left panel for $B_0 = 100\mu$G.

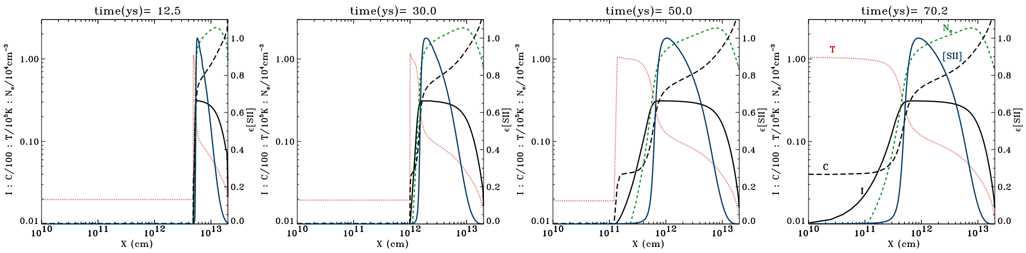

Fig. 2. Evolution towards the steady-state: the four panels show four different distribution of the quantities given in Fig. 1 for $B = 0$, at different times

the jets kinetic energy to convert into heat is certainly appealing, however until now there is no physical explanation about if and how this process can be at work in YSO jets. Velocity fluctuations may possibly steepen into shock and dissipate their energy to heat the gas but one must consider that radiative losses come into play and act against the the heating process.

An alternative explanation, adopted by C. Lavalley-Fouquet et al. (2000) to interpret the line ratios of DG Tau (see also Hartigan (2004)), is that one observes post-shock regions of high excitation consistent with a filling factor of $\sim 1\%$. Arrays of stationary shocks (see Hartigan, Morse & Raymond, 1994) displayed along the jet with different shock velocities would be able to reproduce the observed line ratios.

The problem is how one can actually produce shocks along the jet. The simplest possibility is to start from velocity perturbations that evolve into shocks. In this paper i) we obtain the spatial distribution of the physical variables in the post-shock region for HD and MHD stationary shocks, ii) verify that our

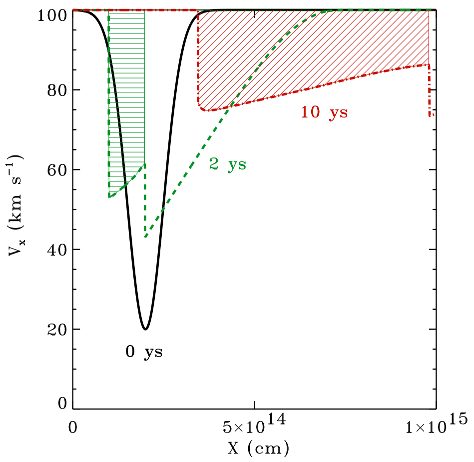

Fig. 3. Temporal evolution of a Gaussian velocity perturbation. The shaded parts are the post-shock regions considered for the evolution.

time-dependent code asymptotically reproduce stationary behavior, and iii) discuss how a, initially strong, planar perturbation can evolve into shocks as it travels along the jet, obtain the behavior of the post-shock values at different evolutionary times, and compare the resulting line ratios with observations.

2. Stationary shocks

Our goal is to consider the temporal evolution of planar perturbations that evolve in radiative MHD shocks. We proceed examining as a first step the stationary case (see Hartigan et al., 1994) for obtaining the spatial evolution of the post-shock physical quantities. We integrate the steady-state MHD Euler equations with cooling: the continuity, momentum conservation and induction equations are solved to yield the three integration constants C_0, C_1, C_2:

$$\rho v = C_0 \quad (1)$$
$$C_0 v + p + 1/2 B_y^2 = C_1 \quad (2)$$
$$v B_y = C_2 \quad (3)$$

The remaining ordinary differential equations of energy and of the fraction of neutral hydrogen atoms f_n must be solved numerically:

$$v\frac{dp}{dx} + \gamma p \frac{dv}{dx} = -(\gamma - 1)\mathcal{L}(T, \rho, f_\mathrm{n}) \quad (4)$$
$$v\frac{df_\mathrm{n}}{dx} = \mathcal{S}(T, \rho, f_\mathrm{n}) \quad (5)$$

The source term

$$\mathcal{S} = n_\mathrm{e}[-c_\mathrm{i} f_\mathrm{n} + c_\mathrm{r}(1 - f_\mathrm{n})]$$

includes collisional ionization and recombination, and where n_e is the electron density c_i and c_r are the ionization and recombination rate coefficients, and $\mathcal{L}$ represents the energy loss term (energy per unit volume per unit time) which includes energy lost in lines and in the ionization and recombination processes. In the radiative losses we include line emission from nine elements, whose abundances have been assumed to be solar: H, He^0, C^0, C^+, N^0, N^+, O^0, O^+, Mg^+, Si^+, S^+ and Fe^+. In this framework we have

$$n_\mathrm{e} = n_\mathrm{H}(1 - f_\mathrm{n}) + Z n_\mathrm{H} \quad (6)$$

where n_H is the total hydrogen density and Z (=0.001) is the metal abundance by number. Expressing ρ, B_y and p as functions of v and f_n:

$$\rho = \frac{C_0}{v}\ ,\ B_y = \frac{C_2}{v}\ ,\ p = C_1 - C_0 v - \frac{1}{2}\frac{C_2^2}{v^2}$$

and differentiating p, we obtain:

$$\frac{dp}{dx} = \left(-C_0 + C_2^2 \frac{1}{v^3}\right)\frac{dv}{dx} \quad (7)$$

$$T = \frac{p\,\mu(f_\mathrm{n})\,m_\mathrm{H}}{\rho k_\mathrm{B}} = \frac{(C_1 v - C_0 v^2 - \frac{1}{2}\frac{C_2^2}{v})\,\mu(f_\mathrm{n})\,m_\mathrm{H}}{C_0}\,. \quad (8)$$

We have solved Eqs. (4) and (5), making use of Eq. (7), for a given set of pre-shock parameters.

The results are shown in Fig. 1, where we plot the post-shock spatial evolution of temperature, electron density, ionization fraction, compression ratio and [SII] emissivity for a hydrodynamic (left panel) and a MHD shock. We note that the post-shock material cools more rapidly in the hydrodynamic case, with

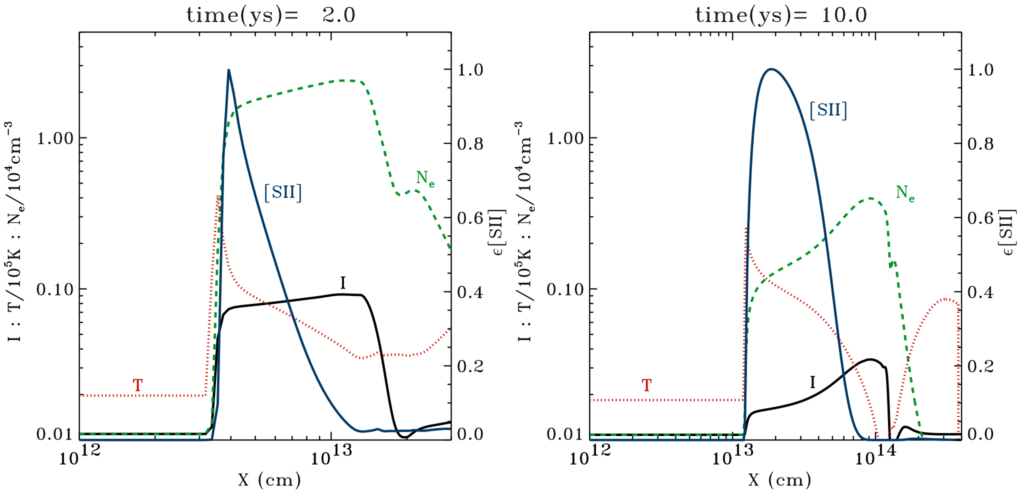

Fig. 4. Left panel: Spatial evolution of the post-shock quantities for an initial gaussian perturbation: temperature (label T), electron density (N_e), ionization fraction (I) and emissivity in the [$S\,II$] line, scaled to the maximum value. The perturbation velocity amplitude is $V_s = -80$ km s^{-1} and the upstream values are temperature $T_0 = 2,000$ K, density $N_0 = 10^4$ cm^{-3}, ionization fraction $I = 0.01$ and magnetic field $B_0 = 100$ G. Snapshot after 2 ys of evolution. Right panel: The same as in the left panel after 10 ys.

respect to the MHD case, with a higher electron density a shorter cooling distance, and the post-shock pressure is entirely supplied by particles. In the MHD case, magnetic field contribute to the post-shock pressure at temperatures $\lesssim 10^4$ K, thus the electron density does not rise as in the hydro case, compare the different compression ratios, and the cooling distance becomes larger (see Hartigan et al., 1994).

3. Time-dependent shocks

We have solved the MHD equations in 1D, including radiation losses employing the numerical code PLUTO (Mignone & Bodo 2004). As mentioned before, we have first verified that the time-dependent solutions asymptotically approach the steady state described in the previous Section. We have done this in two ways: first, we have taken the steady state solution as initial condition for the time-dependent code and verified that it remained steady and, second, we have impressed on the right boundary values obtained from the stationary solution at a given distance from the shock and let the system evolve to eventually reach the steady state solution.

We succeeded in both cases, and results from the second test are given in Fig. 2 where we plot the physical quantities of Fig. 1 at four different evolutionary times for the case of $B = 0$: we note that the post-shock quantities indeed asymptotically reach the stationary behavior.

We then examine the evolution of a isobaric velocity perturbation, that conserves the momentum flux ρv =constant. The initial perturbation shape is a Gaussian with amplitude of 80 km s^{-1} and is negative with respect to the mean jet flow. The evolution of the perturbation is studied in a reference frame where the perturbation remains approximately at rest. In Fig. 3 we show how the perturbation evolves into a forward and reverse shocks (see Hartigan & Raymond 1993), and the shaded zones are the post-shock regions we are going to examine. We notice that the shock velocity of the forward shock is $\sim$ 45 km s^{-1} after 2 years and drops to $\sim$ 25 km s^{-1} after 10 years of evolution. In Fig. 4, similarly to the station-

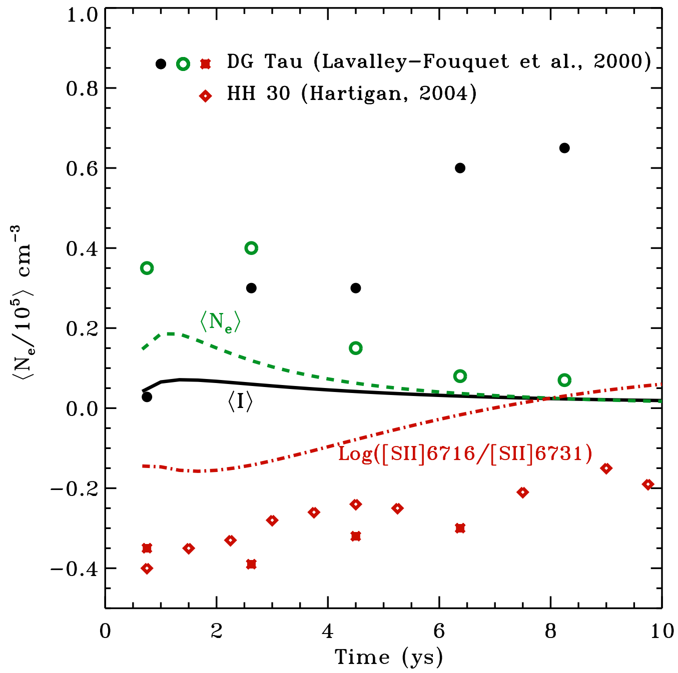

Fig. 5. Temporal evolution of the [SII]-weighted post-shock quantities: electron density $\langle N_e \rangle$ (dashed line), ionization fraction $\langle I \rangle$ (solid line) and line ratio of $[S\,II]\lambda 6716$ to $[S\,II]\lambda 6731$ (dot-dashed line). Symbols represent observed $[S\,II]_{\rm ratio}$ for HH30 and DG Tau jets, electron density and ionization fraction of the HV component of the DG Tau jet, after assuming a jet velocity of 200 km s^{-1}.

ary case, we show the post-shock temperature, ionization fraction, electron density and $[S\,II]$ emissivity after 2 and 10 years of evolution for $B = 100\ \mu$G, $N = 10^4$ cm^{-3} and the same preshock values as in the stationary case. The post-shock region extends $\sim 4 \times 10^{13}$ cm after 2 years and $\sim 3 \times 10^{14}$ cm after 10 years. We must take into account, however, the presence of the post-shock region of the reverse shock, partially shown in the right part of Fig. 4.

In order to carry out a comparison with observations, albeit still partial and limited to a single perturbation, we follow Hartigan et al. (1994) and define the $[S\,II]$-weighted as follows

$$\langle Q \rangle = \frac{\int Q(x)\epsilon\{[S\,II](x)\}\,dx}{\int \epsilon\{[S\,II](x)\}\,dx}$$

where Q is a physical quantity such as density, ionization fraction, etc.; we also define the emissivity ratio of the $[S\,II]$ doublet as

$$[S\,II]_{\rm ratio} = \frac{\int \epsilon\{[S\,II]6716(x)\}\,dx}{\int \epsilon\{[S\,II]6731(x)\}\,dx}\ .$$

Assuming a jet velocity of 200 km s^{-1}, we can translate the observed line ratios along the jet into values in time and make the comparison with the results of the calculation. In Fig. 5 we show the behavior of the $[S\,II]$-weighted electron density and ionization fraction and the $[S\,II]_{\rm ratio}$ vs time. Symbols represent the observed $[S\,II]_{\rm ratio}$, electron density and ionization fraction for the DG Tau and HH 30 jets. Comparing the computed with the observed values of $[S\,II]_{\rm ratio}$ we note that there is typically a discrepancy of, at least, a factor of two.

Moreover, examining the electron density and the ionization fraction from the shock model and comparing these values with those derived from observations we notice a substantial difference. This implies that a decreasing shock strength, even starting with a perturbation velocity that is a substantial fraction of the jet speed, cannot reproduce the observed values.

4. Conclusions

The line emission observed in the first few arcseconds of many Herbig-Haro jets can be interpreted in terms of stationary shocks with velocities 50-100 km s^{-1} (e.g. Lavalley-Fouquet et al. 2000). When shocks are obtained starting from velocity perturbations in the same range of amplitudes and the temporal evolution of the post-shock regions is examined, the resulting values do not match observations. Thus stronger initial pertubations are needed. These conclusions are still preliminary and based on a limited parameter space analysis. However, one must note that both the planar-shock approximation and the choice of a isobaric and flux-conserving perturbation are most favorable for the evolution of strong and persistent shocks.

We plan, before going to consider the 2D case, to carry out a more extensive analysis of the pre-shock parameter space and to impose initial perturbations of different strength and structure, for looking whether a shocking jet can explain observations.

Acknowledgements. The authors thank Sylvie Cabrit and Pat Hartigan for discussions and comments and Francesca Bacciotti for suggestions.

References

Bacciotti, F., Eislöffel, J., Ray, T.P, 1999, A&A 350, 917
Bacciotti, F., Eislöffel, J., Ray, T. P., Mundt, R., Solf, J., 2004, A&A, in press
Hartigan, P., Raymond, J., 1993, Ap.J. 409, 705
Hartigan, P.,Morse, J. A., Raymond, J., 1994, Ap.J. 436, 125
Hartigan, P., Paper presented at the Banff Conference on:*Cores, Disks, Jets & Outflows in Low & High Mass Stars Forming Environments*, July 2004
Lavalley-Fouquet, C., Cabrit, S., Dougados, C., 2000, A&A 356, L41
Mignone, A., Bodo, G., 2004, in preparation
O'Brien, D., Garcia, P., 2003, APSS 287, 3
Rossi, P., Bodo, G., Massaglia, S., Ferrari, A., 1997, A&A 321, 672
Shang, H., Glassgold, A. E., Shu, F .H., Lizano, S. 2002, ApJ 564, 853